Simulation of Bond Coat Properties in Thermal Barrier Coatings During Bending

Nilima Roy[a], Kersi M. Godiwalla[a], Satyabrata Chaudhuri[b] and Ashok K. Ray[b]

[a]*CAP Division,* [b]*MTE Division, National Metallurgical Laboratory*
Jamshedpur -831007, Bihar, India.

(Received May 22, 2000; final form July 11, 2000)

ABSTRACT

Analytical models are presented for predicting bond coat properties of thermal barrier coatings (TBCs) during crack propagation studies induced by bending. Studies on crack propagation behaviour in TBCs were performed with plasma spray coated zirconia, bonded by a MCrAlY layer to Ni -base superalloys (Inconel 617 and CMSX-4). Such thermal barrier composites are currently considered as candidate materials for advanced gas turbine stationary components. Coating as a protective layer improves the surface properties of the substrate. At a temperature of 1073 K, the crack propagation was found to be confined to the TBC (ceramic layer), as the ductile bond coat offers an attractive sink for stress relaxation. The stress-strain behaviour is a function of the elastic modulus of coating, bond coat as well as that of substrate. Thus, from a knowledge of the elastic modulus of TBC and that of substrate, the elastic modulus of the bond coat needs to be evaluated which is a basic parameter for characterizing coating performance. In this paper, the elastic modulus of the bond coat has been determined by modifying the existing model for a two-layered composite beam to a three-layered composite beam.

Key Words: Analytical model, Crack propagation, thermal barrier coatings (TBCs), Ni- base super alloy, gas turbine components, bond coat, layered composite beam.

1. INTRODUCTION

TBCs represent an attractive materials approach of enhancing the high temperature limits for systems such as gas turbines, aircraft engines and diesel engines. Industry and academia in the recent years are actively pursuing research on evaluating the lifetime and thermomechanical behaviour of candidate materials in turbine blades and vanes being subjected to high mechanical stresses and aggressive environments /1-11/. These blades and vanes are made of superalloys with ceramic thermal barrier coatings (TBCs).

The Ni-base superalloys which have been developed for this application are made of superalloys having a γ matrix (solid solution based on nickel) strengthened by both solid solution and precipitation of the γ'-Ni_3 (Ti,Al) phase. The demand for higher efficiencies and durability has resulted in directionally solidified alloys, single crystals, alloys strengthened by oxide dispersion (ODS) or by carbide fibres /1/. Crack propagation studies and failure modes of TBCs on (i) Ni-base superalloy having a γ' phase > 50% /2/ and (ii) Inconel-617 under bending for gas turbine vanes have been studied and reported elsewhere /2,3/. The significant differences in properties between ceramic and metal, as well as the severe temperature gradients applied in such systems, cause thermal stresses that can lead to cracking, delamination and ultimately spalling of the coating. It was established that under conditions simulating jet engine applications /4-5/, one significant contributor to such spalling is oxidation of the bond

coat. Many studies have concentrated on the time to spalling as a function of heat flux /6-9/ and as a function of surface stresses and crack tip opening /9/.

Zirconia partially stabilized by 6-8 wt% yttria seems to be a reasonable material for TBC /1/. However, the behaviour of TBC in a corrosive environment especially in the presence of vanadium is not entirely satisfactory /1/. In addition, a NiCrAlY or NiCoCrAlY type metallic undercoat insures the bonding and the adherence of the thermal barrier on the substrate and also improves the corrosion resistance of the substrate. The mechanical integrity of the bond coat is related to its properties. The ductility of the bond coat is most important. Ductility is generally quantified by the strain energy necessary for the initiation of the first crack in a coated material using bending or tension tests /1/.The elevated temperature tests reveal that above a certain temperature the bond coat is ductile since the strain to cracking increases rapidly. Thus it is possible to predict a ductile to brittle transition temperature (DBTT) for the bond coat which depends on the thickness of the bond coat as well as the Al content /1/. When the components are subjected to severe thermomechanical cycles, MCrAlY coating is chosen because of its favourable ductility and thermal expansion coefficient. No quantitative approach for DBTT is really available to date.

In recent years, concentrated efforts have been made to understand the mechanisms of crack initiation and propagation in TBCs under controlled experimental conditions /9-11/. Keeping this in view, an attempt was made to study the crack propagation behaviour in TBCs at room temperature in the as received and oxidized conditions as well as at a higher temperature (1073 K) /2,3/. The aim of the present work is to derive analytical models for predicting the elastic modulus of the bond coat /2,3/ which is a basic parameter for characterising coating performance during crack propagation studies under bending. The existing analysis for two-layered composite beam has been extended to a three-layered composite beam to facilitate prediction of the elastic modulus of the middle layer, namely bond coat.

2. EXPERIMENTAL:

The failure behaviour of the TBC systems was studied in bending tests with in situ observation of the cracking mechanisms /2,3/.

2.1. Material Specification

Ni-base superalloy (a) Inconel-617 from an indigenous source, designated as source A and (b) CMSX-4 from an industrial source, designated as source B containing γ' phase (~67%) were the substrate materials for the TBCs. A NiCrAlY type metallic undercoat or bond coat was first generated by plasma spraying to ensure the bonding and the adherence of the thermal barrier on the substrate and to improve the corrosion resistance of the TBC. Thereafter, zirconia (stabilized with 8 wt% yttria) based thermal barrier coating was plasma sprayed on the bond coat. Although the substrate materials of the TBCs from two different sources were different, the plasma spraying parameters were maintained nearly the same. In the case of bond coat, in order to approach theoretical bulk density and extremely high adhesion strength, plasma spray was carried out in inert gas chamber and at reduced pressure /12/. The powder particles, approximately 40 μm in diameter, were accelerated and melted in the flame on their high speed (100-300 m/s) path to the substrate, where they impacted and underwent rapid solidification (10^6 K/s). The atomizing gas used is Argon, to exclude oxygen from the vicinity of the flame and work piece.

Typical parameters for turbine vane coating in the present investigation are reported in /2,3/.

2.2 Specimen Preparation

From the as received plate-shaped vane components four point bend (FPB) specimens were machined using ultrasonic cutting and spark erosion technique. The height (h), width (b) of the various FPB specimens, along with the thickness of the ceramic layer (d_c) and the thickness of the bond coat (d_b) are listed in Table. 1. Fig.1a shows a schematic cross sectional view of the multi-layered specimens.

2.3 Microstructure

The as received TBC-substrate specimens were first mounted using standard thermosetting resins and then polished manually on emery polishing paper of different

Table 1
Dimension and coating thickness of the TBC specimens for FPB experiments

Type	Source	Test temperature, K	h (mm)	b (mm)	D_c (mm)	D_b (mm)
1. As received	A	RT-298	1.71	2.64	0.60	0.1
2. As received	B	RT-298	1.83	2.61	0.50	0.1
3. Oxidised at 1273 K for 200 hours	A	RT-298	2.42	2.31	0.27	0.11
4. Oxidised at 1273 K for 200 hours	B	RT-298	2.41	2.22	0.30	0.10
5. As received	B	1073	3.00	3.88	0.50	0.20

grits (200, 400, 800 and 1200). This was followed by polishing the mounted specimens with 9μm, 6 μm, 3 μm and then 1μm alumina suspension, cleaning with acetone and drying the specimens. The thickness of the TBC (ceramic layer) and that of the bond coat were measured by optical microscopy. Another set of samples were oxidized at 1273 K for 200 hours at 10^5 Pa, in an Argon / 20 volume % oxygen atmosphere. Prior to the crack propagation tests under four point bending all the samples were polished using a final polishing step with 0.1μm diamond paste. The surface was finally cleaned with acetone and dried. After the FPB tests, the microstructure of the substrate was examined by electrochemically etching the specimens /2,3/. Microstructures revealing the triple point junction (i.e the grain edges at the junction of adjacent grain

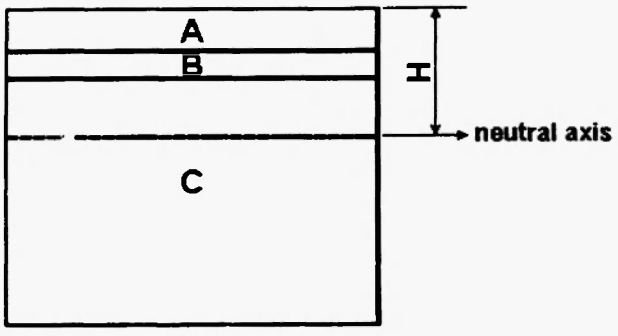

Fig. 1a: Schematic of cross sectional view of a plasma sprayed TBC on Ni base superalloy.
A-TBC (ceramic layer)
B-Bond coat
C-Substrate (Ni base superalloy)
H-Distance of neutral axis from the surface of the TBC.

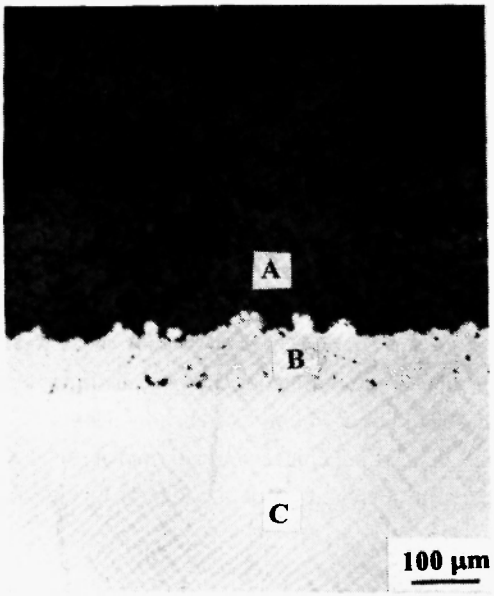

Fig. 1b: Micrograph of a plasma sprayed TBC in as received condition (Type 1, source A). The sample is polished and unetched.
A-TBC (ceramic layer)
B-Bond coat
C-Substrate

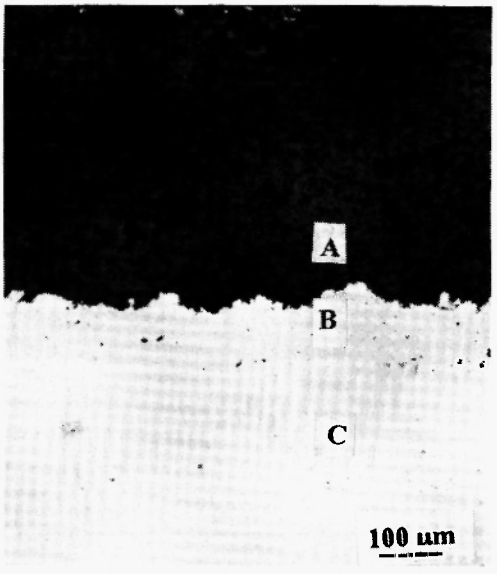

Fig. 1c: Micrograph of a plasma sprayed TBC (Type2, source B). The sample is polished and unetched. The TBC (ceramic layer) has less % porosity and defect compared to the one reported in Fig. 1b.
A-TBC (ceramic layer)
B-Bond coat
C-Substrate

boundaries and the grain boundary precipitates) of the superalloy Inconel-617 in the Type 3 specimen, the γ' phase in the Ni base superalloy from source B, the oxidised sample (Type 4 specimen) and the Al (aluminium) depleted zones just below the TBC and the interface of the coating and the bond coat as well as at the interface of the bond coat and the substrate observed in Type 3 and Type 4 composite beam specimens are all reported in /2,3/. Typical optical micrographs of the specimens in unetched mode are shown in Figs. 1b and 1c.

2.4 Crack Propagation Studies

Crack propagation studies were conducted under four point bend (FPB) loading using a miniature testing device monitored on the stage of an optical microscope (RT tests) and a servohydraulic Instron-1362 machine (for 1073 K test). The TBC (ceramic layer) was on the tensile surface. The ramp rate for loading was maintained at 2.5 Ns^{-1} and the deflection was measured with an LVDT. The load versus deflection curves were recorded as the raw data from each experiment and are reported elsewhere /2,3/. Most of the tests were conducted at room temperature (RT- 298 K), where the bond coat behaves in a brittle manner and few at 1073 K where the bond coat is ductile. Strain values corresponding to deflection were evaluated on the basis of geometric two layer relations using the following equations /13/:

$$\varepsilon = h_o / R \tag{1}$$

$$R = \delta / [1 - \cos(\theta/2)] = \delta / \{1 - \cos[\sin^{-1}(\delta / L/2)]\} \tag{2}$$

where ε is the strain corresponding to deflection δ, L is the difference between the outer and inner span in four point bend loading, h_o is the distance of the neutral axis of the FPB specimens from the interface of the ceramic coating and the bond coat. R is the radius of curvature of the neutral axis due to deflection at an angle θ.

h_o is calculated from the following expression /13/:

$$h_o = \frac{E_s ds^2 - E_c dc^2}{(2 Esds + 2 Ecdc)} \tag{3}$$

where E_s = 210 GPa at room temperature and E_c = 110 GPa at room temperature and E_c = 108 GPa at 1073 K /2/. E_s and E_c are the elastic moduli of the substrate and TBC (the ceramic layer) respectively, d_s and d_c are the thickness of the substrate and the ceramic layer respectively. It is important to note that in this first order approximation, the subtle differences in the elastic properties between the bond coat and the substrate were neglected. The load versus strain and stress versus strain curves of the composite beam specimens are shown in Figs. 2 and 3 respectively.

The TBC inherited many microcracks due to the plasma spraying process, but under bending stresses larger cracks became prominent and grew across the height (thickness) of the specimen. The crack length was monitored microscopically on the side surface of the specimens and was measured with special care in locating the crack tip. The crack path trajectory was

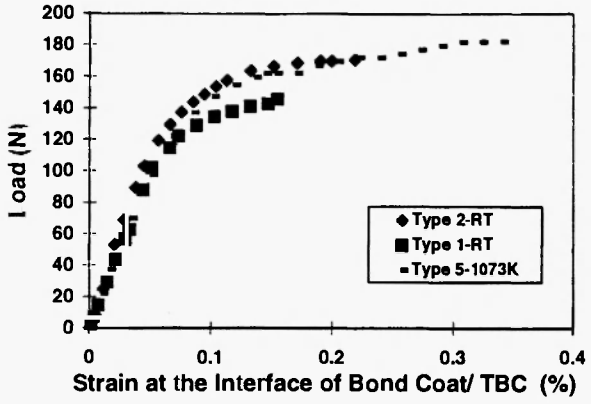

Fig. 2a: Plots of load versus strain at the interface of bond coat/TBC for composite beam specimens – Type 1, Type 2 and Type 5.

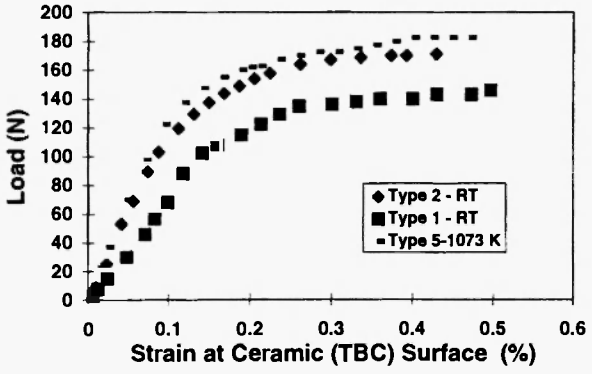

Fig. 2b: Plots of load versus strain at ceramic (TBC) surface for composite beam specimens – Type 1, Type 2 and Type 5.

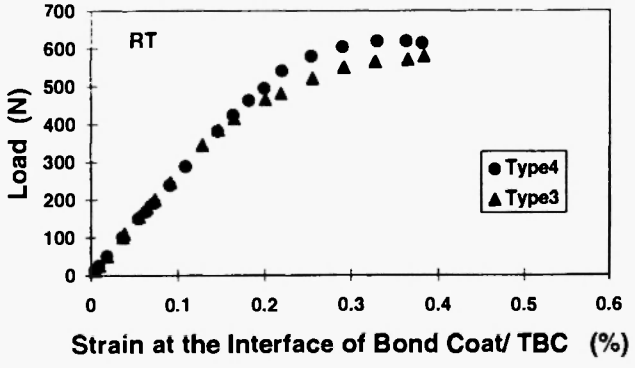

Fig. 2c: Plots of load versus strain at the interface of bond coat/ TBC for composite beam specimens – Type 4 and Type 3.

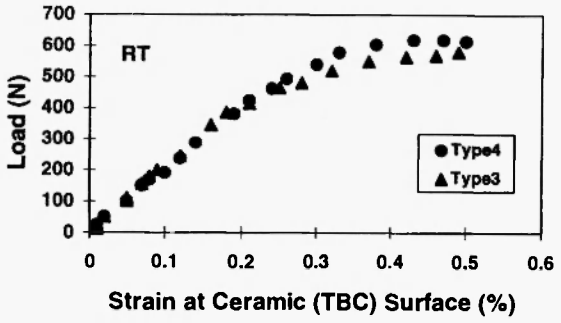

Fig. 2d: Plots of load versus strain at ceramic (TBC) surface for composite beam specimens- Type 3 and Type 4.

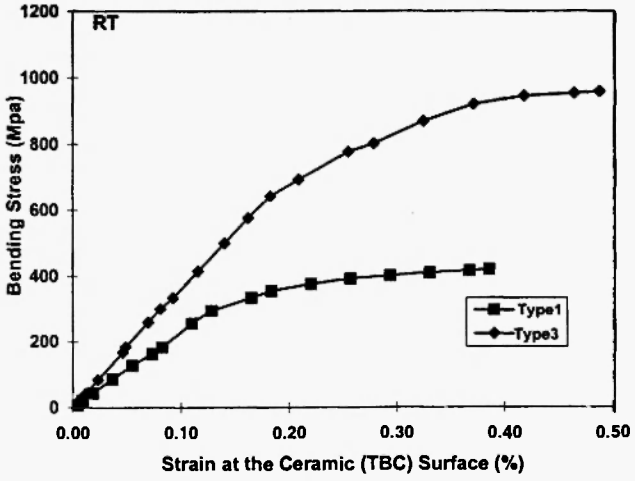

Fig. 3a: Stress versus strain curves for composite beam specimens- Type 1 and Type 3.

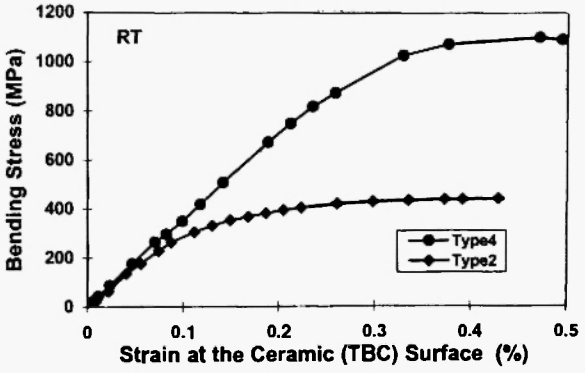

Fig. 3b: Stress versus strain curves for composite beam specimens - Type 2 and Type 4.

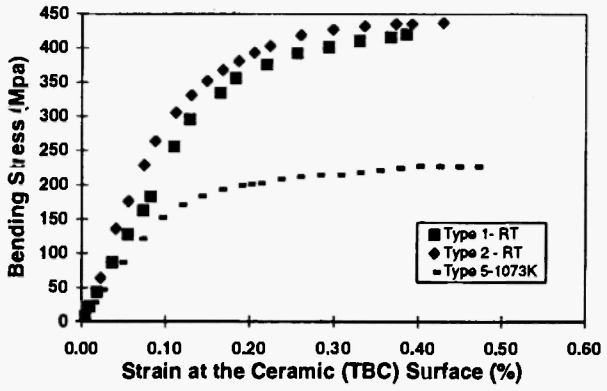

Fig. 3c: Stress versus strain curves for composite beam specimens- Type 1, Type 2 and Type 5.

recorded and printed by a video scanner for RT (298 K) tests and by a sophisticated camera system attached to the microscope for the high temperature (HT = 1073 K) test. The crack extension was correlated to the applied load and corresponding deflection of the composite. Load versus crack length plots and deflection versus crack length plots were generated and they are reported in /2,3/. Subsequently, these deflection values were plotted against their corresponding load values by polynomial of the form, $Y = A + Bx + Cx^2 + Dx^3$ and by resorting to the integral method, the values of the energy, $U = \int Y\, dx$ were evaluated corresponding to each deflection value, enabling plots of **U** versus **a** (crack length). The slope at the various points corresponding to the crack lengths when normalised with respect to the height of the specimen gave the strain energy released with respect to crack extension during bending. The strain energies released at the interface of the ceramic coating and the bond coat and within the bond coat are shown in Table 2.

3. MODELING OF A THREE-LAYERED COMPOSITE BEAM

For crack propagation studies, four point bending was chosen as, in gas turbines, the blades and vanes are often subjected to bending.

If a homogeneous rectangular beam is subjected to symmetrical bending /14/, the neutral axis of the beam coincides with the centroid of the cross section. However, if one of the beam's surfaces is coated with a material of different elastic modulus, the beam is no longer homogeneous and the neutral axis shifts from the centroid of the cross section of the composite beam. Thus an in-plane modulus of the coating was proposed from the shift of the neutral axis /14/. In the bent composite beam, the dependence of the normal stresses σ_c and σ_s (where the subscripts c and s denote the TBC

Table 2
Strain energy values at the interface of bond coat and TBC and in the bond coat of the FPB composite specimens /2/

Type	Source	Test temperature, K	Strain energy released, J/ m^2		% Strain at the interface of bond coat/ TBC
			At the interface of bond coat/ TBC	Within the bond coat	
1. As received	A	RT-298	111×10^4	17.80	~ 0.1
2. As received	B	RT-298	131×10^4	23.07	~ 0.1
3. Oxidised at 1273 K for 200 hours	A	RT-298	182×10^4	15.60	0.2
4. Oxidised at 1273 K for 200 hours	B	RT-298	170×10^4	17.60	0.2
5. As received	B	1073	5.40×10^4	-	0.34

and the metallic substrate respectively) upon the transverse thickness coordinate Y (Fig.4) can be expressed as follows /14/:

$$\sigma_c = E_c Y/R$$
$$\sigma_s = E_s Y/R \quad (4)$$

where R is the radius of curvature of the neutral axis, and E_c and E_s are the elastic moduli of the TBC and the substrate. From the equilibrium of the axial forces, the following equation has to be satisfied /14/:

$$\int_{-h_o}^{d_s - h_o} \sigma_s \, dA + \int_{-h_o - d_c}^{-h_o} \sigma_c \, dA = 0 \quad (5)$$

where A is the cross-sectional area. Substituting eqn. (4) into eqn. (5) yields h_o as given in eqn. (3). However, for calculation of strain in the ceramic layer, H was taken into consideration instead of h_o, where

$$H = h_o + d_c \quad (6)$$

The strain at the TBC (the ceramic layer) and at the interface between bond coat / TBC are displayed for as received (RT test), oxidized condition (RT test) and at high temperature-1073 K test (Fig. 2). The results are compatible with those reported for similar TBCs in bend tests /1,7/.

The elastic modulus of the three layered composite beam can be calculated by modifying and generalising the method developed by Chiu *et al.* /13/. Following /13/, the expression for H', which is the distance of the neutral axis from the bond-substrate interface (Fig. 5), has been derived as follows:

$$H' = d_s - \frac{K}{1+K}(d_b + d_c + d_s) \quad (7)$$

where $K = -\frac{\epsilon_s}{\epsilon_c}$

The strain in substrate, $\varepsilon_s = \frac{Y}{R}$. In our calculations, the elastic strain in the substrate is taken into consideration. The normal stress σ_c, σ_s and σ_b of the bent composite beam is described in /14/

$$\sigma_c = \frac{E_c Y}{R}$$
$$\sigma_s = \frac{E_s Y}{R} \quad (8)$$
$$\sigma_b = \frac{E_b Y}{R}$$

where Y is transverse coordinate from the neutral axis, R is radius of curvature of the neutral axis and E_c, E_s and E_b are elastic moduli of the ceramic, substrate and bond coat respectively.

For a three layered composite beam, the equilibrium of axial forces is:

$$\int_{H'-d_s}^{H'} \sigma_s \, dA + \int_{H'}^{H'+d_b} \sigma_b \, dA + \int_{H'+d_b}^{H'+d_c+d_b} \sigma_c \, dA = 0 \quad (9)$$

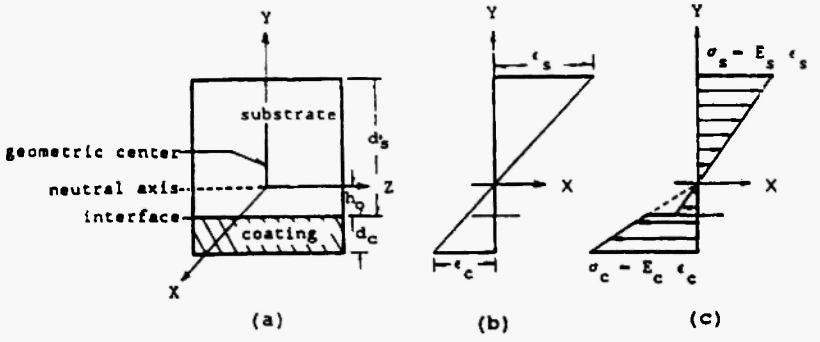

Fig. 4: Stress- strain relationship in a composite beam subjected to a pure bending moment: (a) cross - section of the composite beam; (b) strain development in the axial direction; (c) stress in the axial direction /13/.

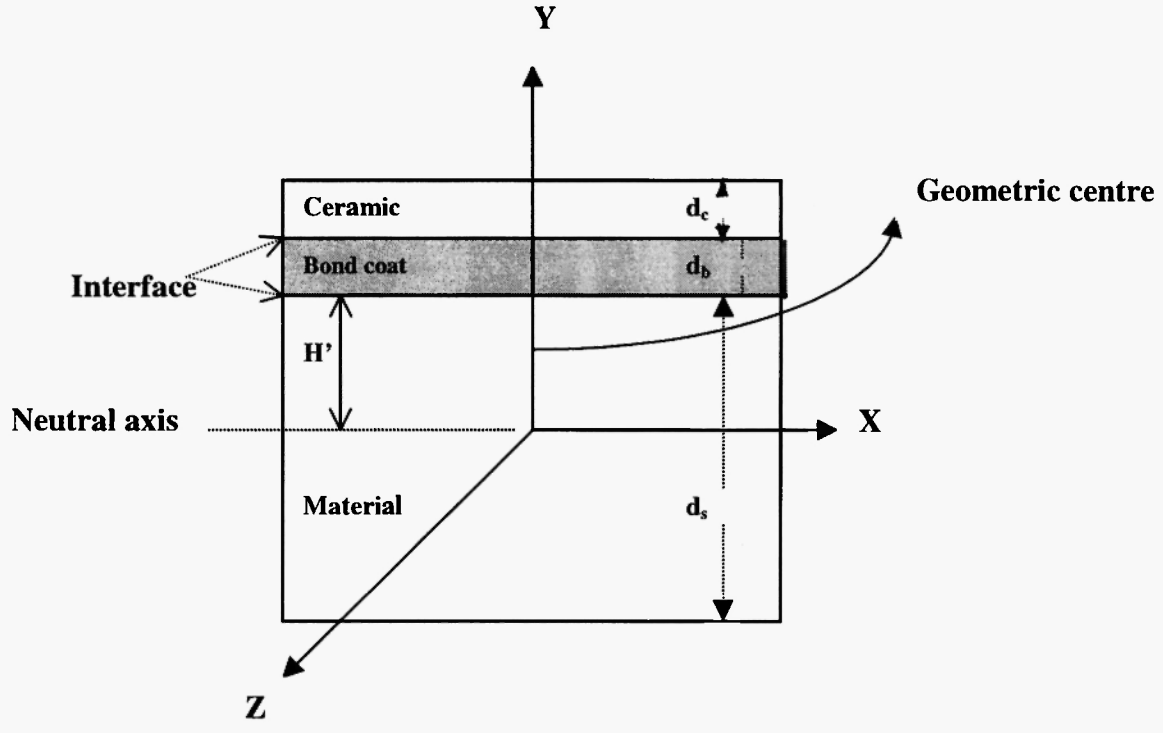

Fig. 5: Cross section of the three layered composite beam in the present investigation subjected to a pure bending moment. H' is the distance of the neutral axis from the interface of bond coat and substrate; d_s, d_b and d_c are the thickness of substrate, bond coat and ceramic layer (TBC) respectively.

where A is the cross sectional area.

From equations (8) and (9), we have

$$H' = \frac{E_s d_s^2 - E_b d_b^2 - E_c d_c^2 - 2E_c d_c d_b}{2(E_s d_s + E_b d_b + E_c d_c)} \quad (10)$$

Equations (7) and (10) yield:

$$E_b = \frac{E_s R_1[2K(1+R_2) - R_1(1-K)] + E_c R_2[R_2(1-K) + 2(1+R_1)]}{[(1+2R_1) - K(1+2R_2)]} \quad (11)$$

where

$$R_1 = \frac{d_s}{d_b}$$

and

$$R_2 = \frac{d_c}{d_b}$$

The value of E_s at room temperature, in oxidised condition and at 1073 K is determined from the slope of the elastic region of experimentally determined stress-strain curves. In these curves, the % strain at the bond coat/TBC interface was plotted against the corresponding bending stresses for the composite beam specimens.

4. RESULTS AND DISCUSSION:

4.1 Metallographic Studies

Micrographs of plasma sprayed TBC substrate (Type 1 and Type 2) are shown in Figs. 1b and 1c respectively, which reveals that the % porosity (~30%) in Type 1 specimen is more than that in Type 2 specimen (% porosity being 18 to 20 %). Further, it was evident that the bond coat also possessed considerable porosity as defects incorporated from plasma spraying, although in Type 2 specimen it was lower.

4.2. Mechanical Properties and Crack Propagation Behaviour of the TBCs

Taking into account the relative mechanical properties of the superalloy and the coating, the latter has a low strength due to the numerous defects and a lower elastic modulus and the (system alloy + coating) can be considered as a composite in which the load bearing contribution of the coating is negligible /1/. If the coating formation involves consumption of alloys as in the case of aluminides and induces a reduction of alloy section, it is necessary to consider the residual section of superalloy for the determination of the effective mechanical stress /1/. This is of particular importance in the case of cooled blades with thin wall sections. On the other hand, for overlay coatings as in the present case, there is no reduction in the load bearing section (eventually a very small reduction, due to interdiffusion effects during the heat treatment applied to improve adherence). These coatings introduce a marginal mass subjected to centrifugal stresses for the blades. As a point of interest, it was found /1/, that for both types of coatings, the ratios of the total section of the component accounting for the stress due to centrifugal loads to the actual load bearing section (alloy) were found to be quite comparable. Therefore in the present investigation, it was assumed that the load is borne by the superalloy substrate and not by the coating. From the load-deflection curves of the bent composite beam, the bending stresses were evaluated without the TBC (ceramic layer) using the standard formula as per ASTM STP 410, for four point bend loading of miniature specimens. The bending stresses at the yield point were 296 MPa, 300 MPa, 693 MPa and 700 MPa for Type 1, Type 2, Type 3 and Type 4 materials respectively (Fig. 3). The stress values for the as received material tested at room temperature are quite compatible to the values reported in literature for Inconel 617 and CMSX-4. It was found that the bending stresses at the yield point of the oxidized specimens were about 2.3 times higher than those of the as received specimens. This could be attributed to microstructural toughening due to solid solution precipitation of massive γ' and γ phases after the Al depleted zone following the bond coat in the substrate of Type 4 specimen /2/ and also owing to carbide precipitation at the bond coat/ substrate interface, grain boundary precipitation and coarsening of grains in the substrate of Type 3 specimen /3/.

The values of E_s and ε_s are tabulated in Table 3. The predicted E_b values from equation (11) are tabulated in Table 4. These E_b values are comparable to the reported E_b values for bond coat of the type Ni18Cr12AlY /15/. From the results it is apparent that the E value predictions of the bond coat compare well with experimental determinations reported in literature, for tests conducted at room temperature /15/. However, a minor deviation was obtained in the case of bend tests at high temperature.

Table 2 reveals the strain energy values at the interface of the ceramic layer and the bond coat and within the bond coat. These values infer that for the oxidized sample a higher strain energy is required for

Table 3
Values of ε_s and E_s determined from experimental data

Type	Source	Test temperature, K	%Strain in substrate (ε_s)	Young's modulus of substrate (E_s), GPA
1. As received	A	RT-298	0.018	210
2. As received	B	RT-298	0.0282	210
3. Oxidised at 1273 K for 200 hours	A	RT-298	0.064	206
4. Oxidised at 1273 K for 200 hours	B	RT-298	0.0652	204
5. As received	B	1073	0.030	200

Table 4
Predicted Young's modulus of the bond coat from the analytical model

Type	Source	Test temperature, °C	Predicted Young's modulus of bond coat (E_b), Gpa	Reported value of E_b from literature /15 / for Ni18Cr12AlY type bond coat, GPa
1. As received	A	RT-25	209	206
2. As received	B	RT-25	209.17	
3. Oxidised at 1273 K for 200 hours	A	RT-25	207	204
4. Oxidised at 1273 K for 200 hours	B	RT-25	206	
5. As received	B	800	182.6	175

the crack to penetrate the bond coat compared to the as received TBCs and this is also probably due to microstructural toughening of the oxidized sample as has been discussed above. Earlier work /16/ had reported room temperature impact toughness of 200 x 10^4 J/m^2 for Inconel 617. Due to the differences in the crack tip loading rates i.e. due to dynamic effects the impact toughness value of Inconel 617 reported /16/ at room temperature is higher than the strain energy released at the bond coat/TBC interface in monotonic loading for as received FPB composite specimens in the present investigation.

For growth of stable cracks in brittle materials (e.g. ceramics, bond coat), notched and precracked specimens are usually desired. In the present situation, the TBC (ceramic layer) already has flaws like microcracks and porosities. Application of load generates stable crack extension because several sources of energy dissipation become activated, e.g. crack deflection, crack arrest in pores, crack bridging and further micro cracking. The crack path trajectory recorded and printed by a video scanner for RT tests and by a sophisticated camera system attached to the microscope for 800°C tests is shown in Figs. 6-9. The crack propagation behaviour of the ceramic thermal barrier coatings (TBCs) at room temperature in as received and oxidised conditions revealed /2,3/ that cracks grow linearly in the TBC with increase in

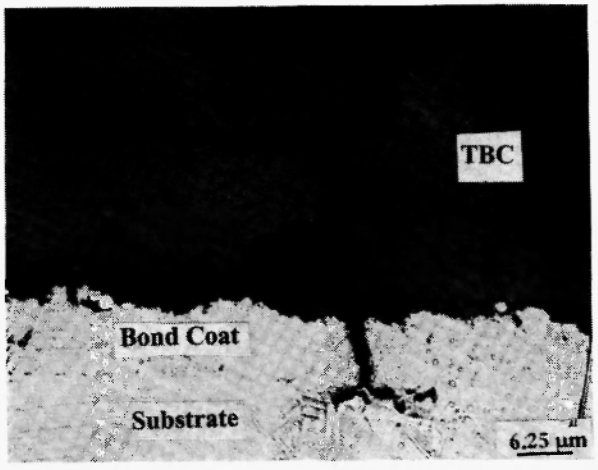

Fig. 6a: Typical crack path trajectory in the TBC (ceramic layer) and in the bond coat in crack propagation studies under bending at RT of Type 2 (source B) composite beam specimen. Crack branching in the TBC, crack tip blunting at the interface of bond coat/substrate and the presence of deformation twins are revealed in the substrate.

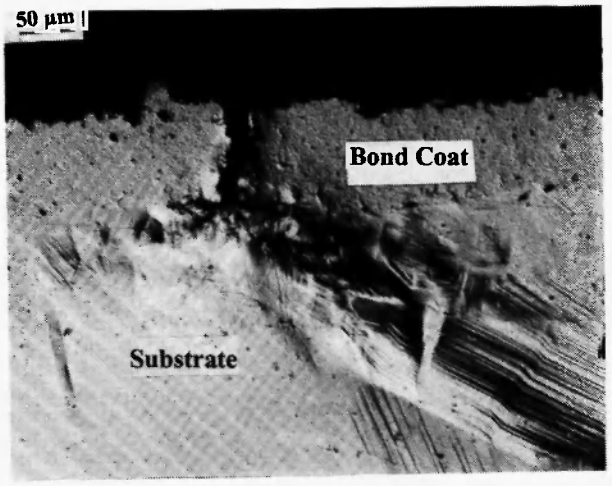

Fig. 6b: The TBC (ceramic layer) has spalled at a deflection 1150 µm in crack propagation studies of Type 2 (source B) composite beam specimen, at RT. The crack front is seen to penetrate more or less vertical into the bond coat. Crack tip blunting at the interface of bond coat/ substrate and a huge plastic deformation is seen in the substrate.

bending load until about the yield point of the superalloy is reached. Approaching the interface between the TBC and the bond coat, a high threshold is required to propagate the crack further into the bond coat. Once the threshold is surpassed, the crack grows rapidly into the brittle bond coat without an appreciable increase in the load /2,3/. It clearly infers that as the crack front penetrates the bond coat, there is a substantial amount of deflection with propagation of the crack within the bond coat, indicative of enormous plastic deformation ahead of the crack front at the bond coat/substrate interface and formation of deformation twins in the metal substrate in the RT tests (see Figs. 6b and 7c). The crack front also revealed blunting of the

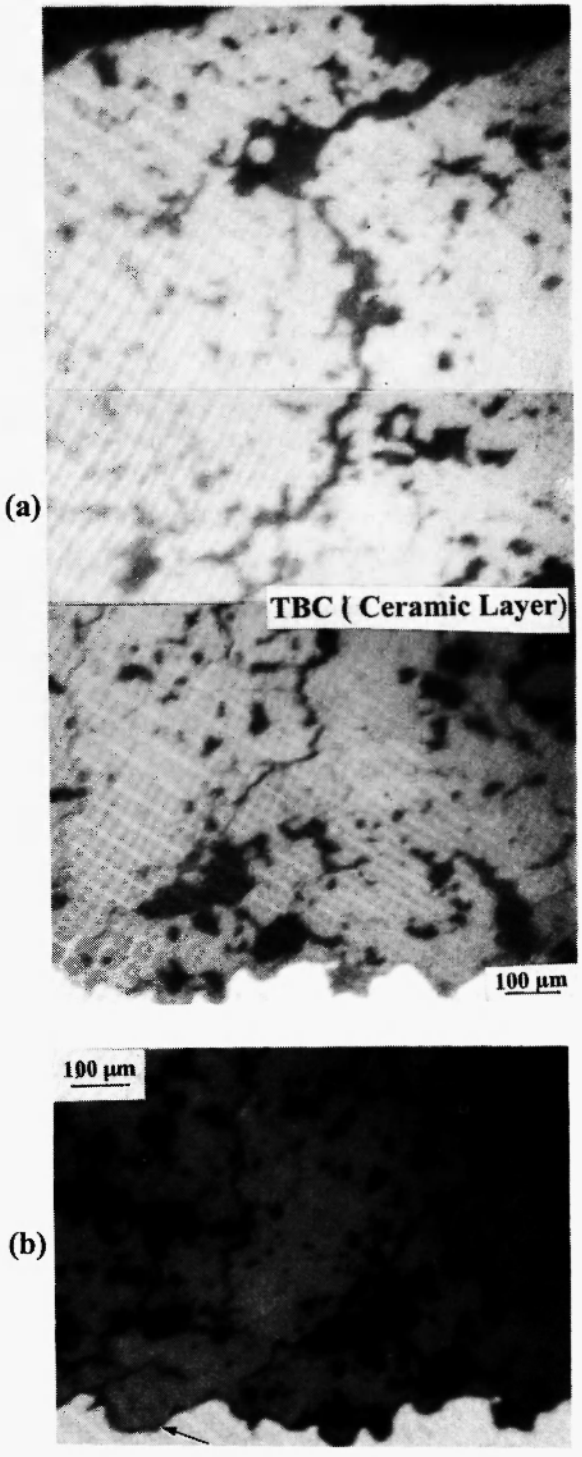

Fig. 7: Typical crack path trajectory in crack propagation studies under bending at RT for Type 4 (source B) composite beam specimen in heat treated condition (oxidised at 1273 K for 200 hours).

(a) Crack propagation in the TBC. The crack is found to initiate from a surface pore in the TBC. The crack frequently branches in the TBC.

(b) The crack front penetrates the Al_2O_3 layer at the interface of TBC/ bond coat and then into the bond coat. Arrow indicates the Al_2O_3 layer.

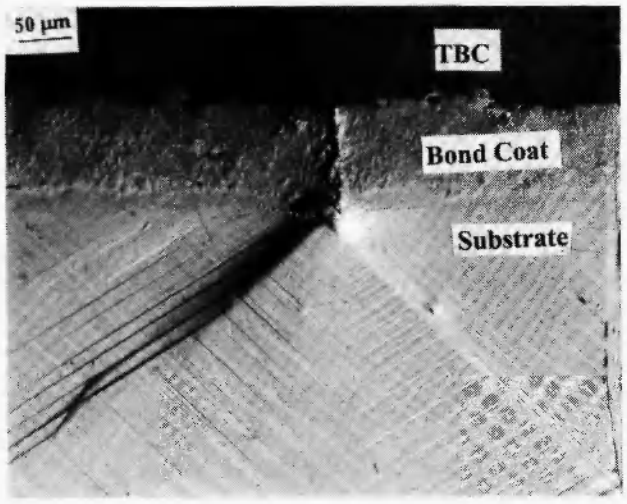

Fig. 7c: Crack path trajectory in the in the bond coat in crack propagation studies at RT of Type 4 (source B) composite beam specimen in heat treated condition (oxidised at 1273 K for 200 hours). The crack front penetrates vertically into the bond coat from the TBC (top most layer). The substrate reveals substantial deformation twins.

crack tip at the bond coat/substrate interface indicative of high ductility of the material. It also implies that the crack, to propagate further in the substrate, requires a very high bending load. At 1073 K, the crack is found to propagate only in the TBC (Figs.8 and 9), as the ductile bond coat protects the metallic component from thermal loads, offers an attractive sink for stress relaxation and becomes ductile at high temperature. This is indicative of the high strain (0.34 %) at the interface of bond coat/ TBC at 1073 K compared to the RT bend tests of the composite beam specimens (Table 2 and Fig. 2a). There was no spalling of the TBC for the composite beam specimen from source A, in any of the bend tests at RT and in the high temperature (1073 K) test /2,3/ from both the sources. Effects of bond coat oxidation on crack propagation in the interface regime had been discussed /2,3/.

It is noteworthy that the crack path trajectory in the TBC (ceramic layer) often showed crack branching and crack deflection (Figs. 6a, 7a, 8 and 9). Generally for materials with R- curve type behaviour, this is a well

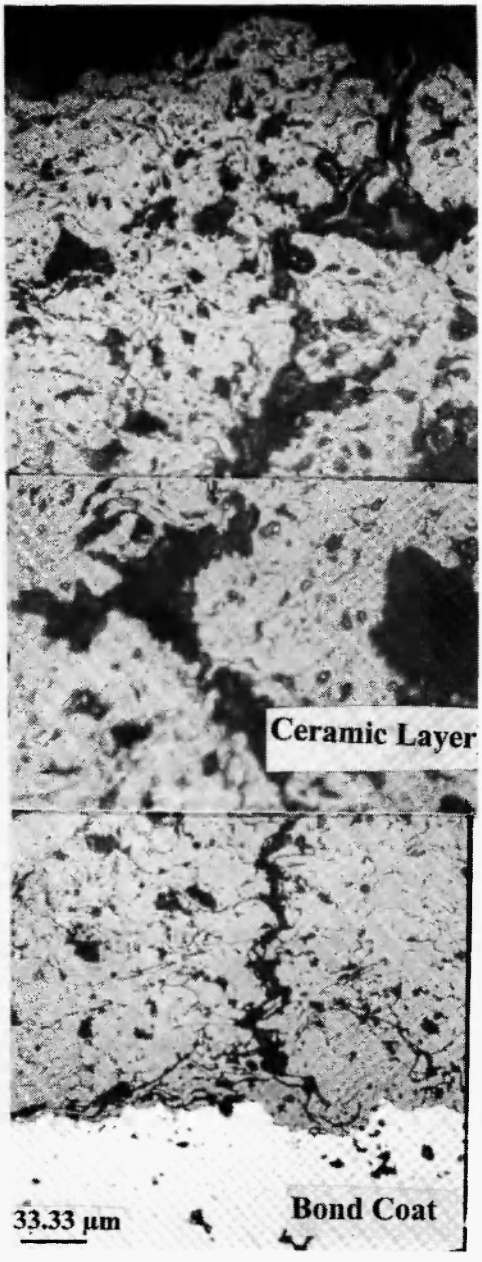

Fig. 8: Typical crack path trajectory in the TBC at 1073 K. Crack growth at 1073 K was confined only to the TBC (ceramic layer).

established phenomenon and it could partly account for the rising trend in the K_R (fracture resistance) values /17-21/. It should also be noted that deformation in the TBC and that in the bond coat pertained to the elastic limit and plastic limit of the load versus deflection curves respectively. Although in the Type 5 composite beam specimen there was a huge deflection (Figs.2a and

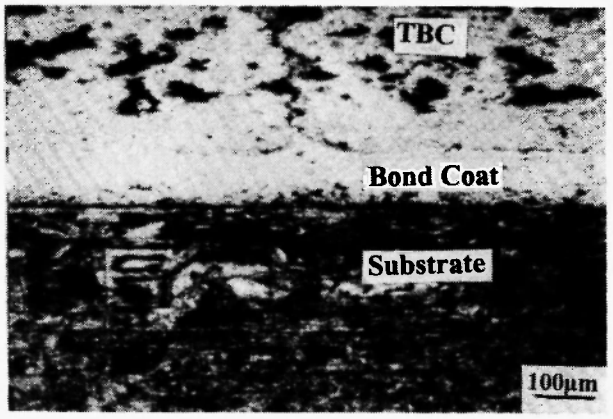

Fig. 9: The in situ micrograph demonstrates that crack propagation at 1073 K was restricted only to the TBC (ceramic layer). This micrograph shows the crack path trajectory of a propagated crack in another region of the TBC /3/.

2b), the crack front never penetrates the bond coat (Figs.8 and 9), as the bond coat is ductile at 1073 K. Therefore in the high temperature (1073 K) test, since the bond coat is ductile and crack propagation is confined only to the TBC (ceramic layer), the strain energy released at the interface of bond coat/TBC was considerably less (5.40×10^4 J/ m^2) as shown in Table 2.

The design process of a TBC needs to establish criteria for acceptability from the point of view of delaying crack initiation and propagation processes. On the other hand, since the function of a TBC is to protect metallic substrates from high temperatures, the thermal resistance of the coating is also an important consideration /11/. Therefore, the design of a TBC is a complex process and one has to consider the thermal loading and other conditions that can be vastly different from one application to another.

5. CONCLUSION

An analytical model for the prediction of elastic modulus of a multi layered beam has been developed. Four point bend test data can thus be used for the theoretical prediction of E values of the bond coat in the bend tests for TBCs conducted experimentally. From the results it is apparent that the E value predictions of the bond coat compare well with experimental determinations reported in literature, for tests conducted at room temperature. However, a minor deviation was obtained in the case of bend tests at high temperature.

ACKNOWLEDGEMENTS:

The data presented in this paper is the outcome of an in house RandD project at NML Jamshedpur on '*Thermomechanical modeling in crack propagation studies of thermal barrier coatings in power plant application*'. The raw experimental data was generated at IWE-1, Forschungszentrum, Jülich, Germany. The authors are grateful to IWE-2, Forschungszentrum, Jülich, for heat treating all the TBCs and for generating some of them. The authors are thankful to IWE-1 for extending all possible help in carrying out the experiments. One of the authors (A.K. Ray) is grateful to DLR Bonn for financial support during the research at IWE-1. Finally, the authors are grateful to Professor P. Ramachandra Rao, Director NML Jamshedpur for permission to publish the manuscript.

REFERENCES

1. C. Duret-Thual, R. Morbioli and P. Steinmetz, *A Guide to the Control of High Temperature Corrosion and Protection of Gas Turbine Materials*, CEC (Commission of the European Communities) COST Energy, EUR 10682 EN, 1986. (Edited by O. Morocutti: Commission of the European Communities, Brussels, Belgium).
2. A.K. Ray, *Int. J. Turbo and Jet Engines*, **17**(1), 1 (2000).
3. A.K. Ray and R.W. Steinbrech, *J. Euro. Ceram. Soc*, **19**, 2097 (1999).
4. R.A. Miller and C.E. Lowell, *Thin Solid Films*, **95**, 265 (1982).
5. W.J. Brindley and R.A. Miller, *Surf. Coat. Technol.*, **43-44**, 446 (1990).
6. R.A. Miller and C.C. Berndt, *Thin Solid Films*, **119**, 195 (1984).
7. C.H. Liebert and R.A. Miller, *Ind. Eng. Chem. Prod., Res .Dev.*, **12**, 334 (1984).

8. J.T. DeMasi, K D. Sheffler and M. Ortiz, *Thermal Barrier Coating, Life Prediction Model Development*, NASA CR 182230, National Aeronautics and Space Administration, Dec (1989).
9. K. Kokini, C.D. Choules and Y. R. Takeuchi, *J. Therm. Spray. Tech. (JTTEE) ASM International*, **6** (1), 43 (1997).
10. L. Lelait, S. Alperine, C. Diot and M. Mevrel,, *Mater. Sci. Eng A.*, **120 –121**, 475 (1989).
11. K. Kokini and Y.R. Takeuchi, *Mater. Sci. Eng. A.*, **189**, 301 (1994).
12. K.H. Stern (Ed.), *Metallurgical and Ceramic Protective Coatings*, Chapman and Hall, 1996; p.266.
13. C.C. Chiu and E.D. Case, *Mater. Sci. Eng A.*, **132**, 39 (1991).
14. S.P. Timoshenko and D.H. Young, *Strength of Materials*, Van Nostrand Reinhold, Princeton, NJ, 4th edn., 1962; p. 113.
15. W.J.Brindley, Jr. *Thermal Spray Technology*, **6** (10), 85 (1997).
16. U. Bruch, D. Schuhmacher, P.J. Ennis and E. Heesen, *Nuclear Technol.*, 66, 357 (1984).
17. N. Ramchandran and D.K. Shetty, *J. Am. Ceram. Soc.*, **74** (10), 2634 (1991).
18. R.M. Anderson and L.M. Braun, *J. Am. Ceram. Soc.*, **73** (10), 3059 (1990).
19. M.V. Swain, *J. Am. Ceram. Soc.*, **73** (3), 621 (1990).
20. G. Pezzotti, I. Tanaka and T. Okamoto, *J. Am. Ceram. Soc.*, **73** (10), 3039 (1990).
21. A.K. Ray, E.R. Fuller and S. Banerjee, *J. Euro. Ceram. Soc.*, **16**, 503 (1996).